Simple Noise Mitigation Scheme for Coherent Optical DMT Signal Transmission System

KE LI[1], TIANYE HUANG[2], (Member, IEEE), ZHONG LIU[1], QIANQIAN LIU[1], YUNLEI ZHANG[1], (Member, IEEE), LIGUO LIU[1], LU LI[3], AND XIANG LI[4]

[1]Electronic Engineering Institute, Naval University of Engineering, Wuhan 430033, China
[2]School of Mechanical Engineering and Electronic Information, China University of Geosciences, Wuhan 430074, China
[3]Optics Valley Technology Stock Company, Wuhan 430200, China
[4]Division of Electrical Engineering, Department of Engineering, University of Cambridge, Cambridge CB3 0FA, U.K.

Corresponding author: Xiang Li (xl470@cam.ac.uk)

ABSTRACT We propose and experimentally demonstrate a noise mitigation scheme for coherent optical discrete multitone (DMT) signal transmission system. The proposed scheme can mitigate the laser phase noise and additive white Gaussian noise (AWGN) simultaneously when optical DMT signal is coherently detected. In the digital signal process (DSP), the laser phase noise is first estimated and compensated through moving average filter. The AWGN is then reduced by considering the time-domain real-valued or frequency-domain symmetrical conjugation characteristic of DMT signal. Finally, we conduct an experiment to transmit dual-polarization (DP-) DMT signal based on a low complexity coherent detection structure with only two pairs of input and output ports. The experimental results prove that the proposed scheme can enhance the signal-to-noise ratio (SNR) and effectively reduce the effect of laser phase noise even the laser linewidth is as large as 10 MHz. The DP-DMT signal is successfully transmitted over 1920-km standard single mode fiber (SSMF) in the experimental demonstration. The analysis of computational complexity also indicates that the proposed DSP scheme requires less number of complex multiplication operations and has larger laser phase noise tolerance than other DSP schemes.

INDEX TERMS Linear phase noise, discrete multitone (DMT), digital signal processing (DSP), coherent detection.

I. INTRODUCTION

With the fast development of design and fabrication techniques, the bandwidth of optoelectronic devices can reach more than 50 GHz, targeting for the baud rate up to 100 GBaud [1], [2]. It is believed that both the channel capacity and data rate per single wavelength have already approached the Shannon limit of the fiber communication system [3]. In the past few days, more attention may have been transferred to find the solutions for low-cost and small-size optical module in the fiber transmission network assuming these high-bandwidth optoelectronic devices are commercially available. In general, low cost means less number of optoelectronic components in the optical module and the size of an optical module is more related to the

number of input and output ports considering the packaging technique. Therefore, intensity modulation and direct detection (IMDD) technique is still popular even though coherent optical modules have been shown much better performances in all levels of fiber transmission networks [4]–[8]. This is mainly because optical module based on IMDD technique is much simpler requiring only 1 pair of input and output port, comparing with 4 pairs of input and output ports in coherent optical module. Based on high-bandwidth Mach-Zehnder modulator (MZM), electrical driver and single-end photodetector (PD), several experimental demonstrations at data rate of 100 Gb/s and 200 Gb/s per wavelength have been reported [9]–[11].

However, the performances of IMDD technique are intrinsically limited in terms of data rate and transmission distance because only one dimension of the signal is transmitted and received. Specifically, the power fading effect will limit

the product of baud rate and chromatic dispersion (CD) if the optical module is operated at C band. The transmission distance is usually less than 40 km if the optical module is operated at O band, because the cost of O-band amplifier is very high and the power loss at O band is large. The common solutions for this issue includes single side-band (SSB) signal generation after optical filtering [12]–[16] and optical pre-CD compensation by dispersion compensation module [17]–[19]. Unfortunately, these solutions will reduce the signal-to-noise ratio (SNR) of transmitted optical signal by introducing additional power loss. Moreover, wavelength division multiplexing (WDM) transmission is also difficult to realize based on these solutions.

Considering the above issues, the structure of intensity modulation and coherent detection (IMCD) has been proposed to reduce the number of input and output ports. Intradyne and heterodyne coherent detection techniques have been experimentally demonstrated for on-off keying (OOK) and 4-level pulse amplitude modulation (PAM-4) formats [20], [21]. It is noted that if the bias point of MZM is set at the linear point, the optical signal contains no phase information, which will not be affected by laser phase noise. In such condition, the optical signal contains optical carrier with large power, which may seriously reduce the effective SNR of the true information. In order to compensate the laser phase noise when the bias point of MZM is set at the null point, conventional carrier phase recovery algorithms designed for quadrature amplitude modulation (QAM) has also been applied for PAM-4 signal [21]. However, these algorithms are only effective when the laser linewidth is smaller than 100 kHz, which cannot satisfy the low-cost requirement if cost-effective distributed feedback (DFB) laser with large linewidth (≥ 10 MHz) is used in coherent detection scheme. Although carrier suppressed PAM-4 signal is recently proposed to overcome the phase noise effect when the MZM is biased at the null point, the associated effective SNR is not increased since the additional coding scheme at the transmitter side transfer the 4-level signal into the 7-level signal [22].

In this paper, we consider the IMCD structure in [23] with two pairs of input and output ports. A digital signal processing (DSP) scheme is designed for discrete multitone (DMT) signal when the bias point of MZM is optimized between linear and null points for carrier phase extraction. Considering the frequency-domain symmetrical conjugation property of DMT signal, the designed DSP scheme can mitigate the effects from both laser phase noise and additive white Gaussian noise (AWGN). We conduct an experiment to transmit and receive 100-Gb/s dual-polarization DMT (DP-DMT) signal with 16-QAM format in heterodyne IMCD structure. By comparing with other existing DSP schemes, the designed DSP scheme shows similar or better performance with the lowest computational complexity. Moreover, the proposed DSP scheme can support the use of low-cost distributed feedback (DFB) laser with linewidth as large as 10 MHz. Based on the designed DSP scheme, the DP-DMT signal is

successfully transmitted over 1920-km standard single mode fiber (SSMF) in the experimental demonstration.

II. PRINCIPLES

The carrier phase extraction scheme for phase noise mitigation of DMT signal is shown in Fig. 1(a). For simplicity, we assume the frequency offset of DMT signal has been compensated with center frequency of zero. In general, the optical carrier can be observed when the bias of MZM is set with a offset to the null point. Since the subcarrier mapping is flexible for DMT signal, the bandwidth of guard band between the optical carrier and information band is adjustable. Therefore, the carrier phase information can be extracted by passing the baseband DMT signal through a digital low-pass filter (LPF) with bandwidth equal or smaller than the bandwidth of guard band. In [24], moving averaging filter (MAF) is proposed for orthogonal frequency division multiplexing (OFDM) format to extract the carrier phase information by assuming the coefficients of digital filters are all ones, as described in Fig. 1(a). In this case, only the length of the digital filter requires optimization, which is related to the bandwidth of guard band. Particularly, if the filter length is equal to the power of 2, the average operation may require no multiplication operation for binary digits, which significantly simplify the DSP scheme. As shown in Fig. 1(a), the output of the digital LPF is then normalized and finally conjugated multiplexed with the input DMT signal to obtain the output DMT signal containing only small residual phase noise. Although the operation principle of carrier phase extraction for DMT is the same as that for OFDM, this method is actually more suitable for DMT. This is mainly because OFDM signal is generated based on IQ modulator. The different bias drift in the I and Q branches will result in amplitude imbalance between the two branches and then affect the system performance.
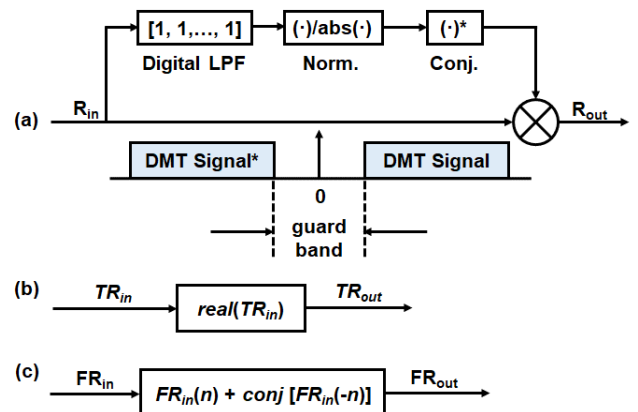

FIGURE 1. (a) Phase noise mitigation scheme based on moving average filter; (b) time-domain noise mitigation scheme by imaginary part removal; (c) frequency-domain noise mitigation scheme by symmetrical conjugation superimposition.

Moreover, we propose to further mitigate the noise effect by considering the symmetrical conjugation property of DMT signal. As described in Fig. 1(b), we can take the $real(\cdot)$

operation to the time-domain sample TR_{in} to remove the imaginary part. This operation is reasonable because the time-domain DMT signal only contains the real part and the imaginary part of DMT signal is introduced by the phase noise and frequency offset. It can be assumed that the imaginary part of DMT signal after frequency offset compensation and phase noise mitigation is only AWGN. Therefore, it is expected that removing the imaginary part of the time-domain DMT signal can reduce the noise power by 3 dB, resulting further performance improvement.

For fair comparison, we also consider scheme to mitigate the noise in frequency domain, as shown in Fig. 1(c). The frequency-domain DMT symbol $\mathbf{FR_{in}}$ after channel equalization should be symmetrically conjugated. It means that the information in the left sideband and right sideband are the same. However, the vector $\mathbf{FR_{in}}$ is no longer symmetrically conjugated if the time-domain DMT symbol is not real-valued due to the introduction of phase noise. It is noted that the noise in the symmetrical part of one frequency-domain DMT symbol is random. Therefore, the noise power can also be reduced by 3 dB when the symmetrically conjugated subcarrier in one frequency-domain DMT signal is superimposed, as also described in Fig. 1(c).

III. EXPERIMENTAL SETUP

We conduct an experiment to evaluate the effectiveness of the proposed noise mitigation scheme. The experimental setup is shown in Fig. 2. The baseband DMT signal is generated offline with fast Fourier transform (FFT) size of 256. The subcarrier index 5 to 80 is mapped with the data symbols, which are encoded by 16-QAM format. In order to realize the real-valued DMT signal, the subcarrier index 178 to 253 are mapped with conjugated data symbols from subcarrier

index 5 to 80. Therefore, 7 subcarriers (1 to 4 and 254 to 256) are left as guard band for carrier phase extraction. The length of cyclic prefix (CP) is 8 to deal with the issue of inter-symbol interference (ISI). The digital baseband DMT signal is then loaded into an Arbitrary waveform generator (AWG) operating at 56 GSa/s and converted to the analog signal. The analog signal is then amplified by an electrical driver with bandwidth of 18 GHz before loaded into the MZM. The transmitter lasers of external cavity laser (ECL) with linewidth smaller than 100 kHz and DFB laser with linewidth around 10 MHz are both considered for completed investigation. The electrical signal is converted to the optical signal in one MZM with bandwidth of 20 GHz, which is biased with a offset to the null point. The single polarized optical DMT signal is then split into two streams by a polarization beam splitter (PBS). One stream is delayed by one DMT symbol and combined with another stream by a polarization beam combiner (PBC) to emulate the polarization multiplexing (PM) process. In our experimental demonstration, the period of one DMT symbol is given by:

$$\frac{1}{56GSa/s} \times (256 + 8) \, Sa \approx 4.7ns \qquad (1)$$

From Eq. (1), we can calculate the delay length as $\sim$0.98 m by assuming the fiber refractive index of 1.44. Therefore, the net data rate considering forward error correction (FEC) code with 20% overhead can be expressed as:

$$\frac{76}{256 + 8} \times 4b/Sa \times 56GSa/s \times 2/1.2 \approx 107.5Gb/s \qquad (2)$$

The generated DP-DMT signal is then passed through an Erbium doped optical fiber amplifier (EDFA), which is used to control the optical power. Next, the amplified DP-DMT signal is launched into the fiber link, which consists of one piece of SSMF with length of 80 km and one Raman amplifier to compensate the power loss. At the receiver side, an optical bandpass filter (OBPF) is first used to mitigate the noise and another EDFA is applied to compensate the power loss. The spectrum of DP-DMT signal at the output of EDFA is shown in the inset (I) of Fig. 2. The local oscillator (LO) at the receiver side has the same type as the transmitter laser (ECL or DFB). A polarization diversity optical hybrid is used to achieve polarization diversity coherent detection. Both the LO and PM-DMT signal are injected into the two input ports of the DP optical hybrid. In order to also simplify the structure at the receiver side, the center frequency of LO is tuned to be 18 GHz away from that of transmitter laser to realize heterodyne coherent detection. Specifically, only two of the eight output ports of the optical hybrid are connected to two single-end PDs instead of two balanced PDs to realize low-complex coherent detection. The bandwidth of the single-end PD is 40 GHz. Therefore, the received signal is actually suffered from signal-to-signal beating interference (SSBI). It is noted that the function of polarization diversity optical hybrid can also be replaced by two PBSs and two polarization-maintaining optical couplers (PMOCs) [23].
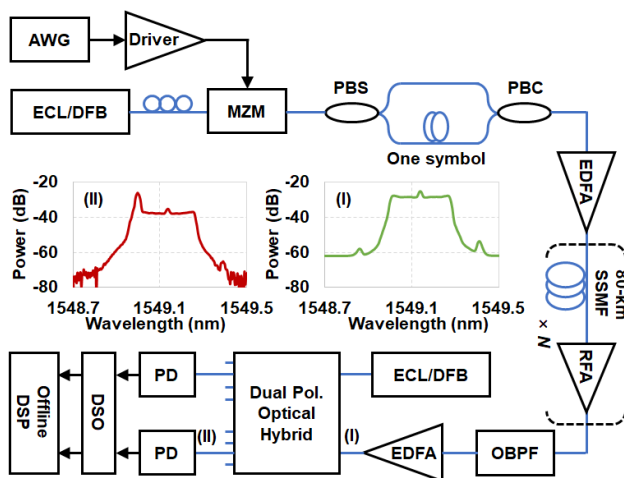

FIGURE 2. Experimental setup of the dual-polarization DMT signal in fiber transmission system based on intensity modulation and coherent detection structure. ECL: external cavity laser, DFB: distributed feedback, AWG: arbitrary waveform generator, MZM: Mach-Zehnder modulator, PBS: polarization beam splitter, PBC: polarization beam combiner, EDFA: Erbium doped optical fiber amplifier, OBPF: optical bandpass filter, PD: photodetector, DSO: digital storage oscilloscope.

In order to achieve the optimal performance, the power ratio between LO and received DMT signal can be adjusted by tuning the output power of EDFA while maintaining the LO power maximized. The optical spectrum of combined LO and DMT signal is shown in the inset (II) of Fig. 2. The leaked optical carrier due to the offset bias value can be observed in both insets of Fig. 2. Finally, the analog signals at the outputs of the two single-end PDs are digitized by one digital sampling oscilloscope (DSO) operating at 160 GSa/s and stored for further processing.

We investigate 5 different DSP schemes to compare their performances, which are described in Fig. 3. It is noted that common DSP steps are applied to all the DSP schemes as pre-processing steps. Among these steps, Kramers-Kronig algorithm is first applied to reduce the effects of SSBI [25]. Then coarse frequency offset compensation (FOC) is performed by directly shifting the 18 GHz frequency offset. Next, the chromatic dispersion is compensated in frequency domain followed by resampling to 1 Sa/s. The fine FOC and time synchronization are finally achieved based on specifically designed preambles [26].
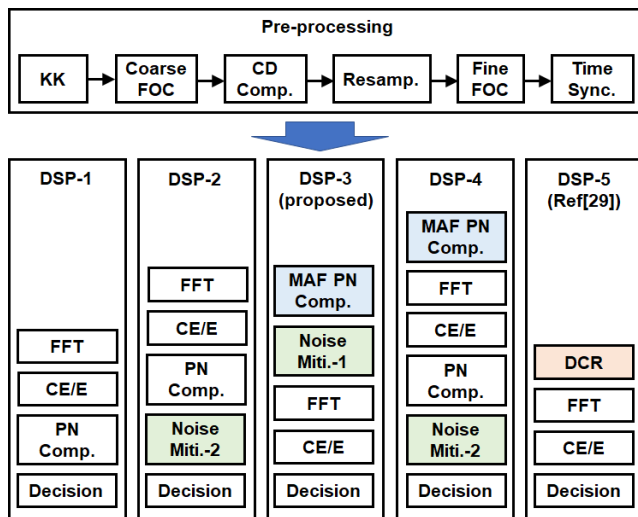

FIGURE 3. 5 different DSP schemes for noise mitigation with same pre-processing steps.

Among the 5 DSP schemes, DSP-1 follows traditional steps including FFT demodulation, training symbols-aided channel estimation/equalization (CE/E) [27], pilot-aided phase noise compensation (PNC) [28] and decision. DSP-2 is only a slightly different from DSP-1 by applying frequency-domain noise mitigation scheme (Noise Miti.-2, described in Fig. 1(c)) after traditional PNC. DSP-3 is our proposed noise mitigation scheme. In DSP-3, MAF-aided phase noise compensation (MAF-PNC, described in Fig. 1(a)) scheme is first applied followed by *real*(·) operation (Noise Miti.-1, described in Fig. 1(b)). Then the normal operations including FFT, CE/E and decision are performed. In DSP-4, MAF-PNC is also used but the Noise Miti.-2 scheme is applied instead of Noise Miti.-1. For comparison, we also consider the digital

carrier regeneration (DCR) scheme as DSP-5 [29], which is based on ideal brick wall filter using the whole length of the signal block. In CE/E process, 20 training symbols are used followed by 300 payload symbols. In traditional PNC scheme, 4 pilots are inserted in each DMT symbol to estimate the phase variation among DMT symbols. One million bits are collected for bit error rate (BER) calculation.

IV. RESULTS AND DISSCUSSION

We first study the carrier phase extraction process by considering the electrical spectrum. The electrical spectrum of DMT signal after fine FOC based on ECL and DFB pairs are shown in Fig. 4(a) and (b), respectively. The guard band can be observed in both cases. The electrical spectrum of samples at the output of MAF for the two cases are shown in Fig. 4(c) and (d). It can be seen that the spectral part of DMT information is significantly suppressed, which means the carrier phase information can be effectively extracted. The enlarge versions of frequency-domain carrier phase information are shown in Fig. 4(e) and (f), respectively. It is also proved that the extracted carrier from DFB pair has larger linewidth or phase noise than that from ECL pair.
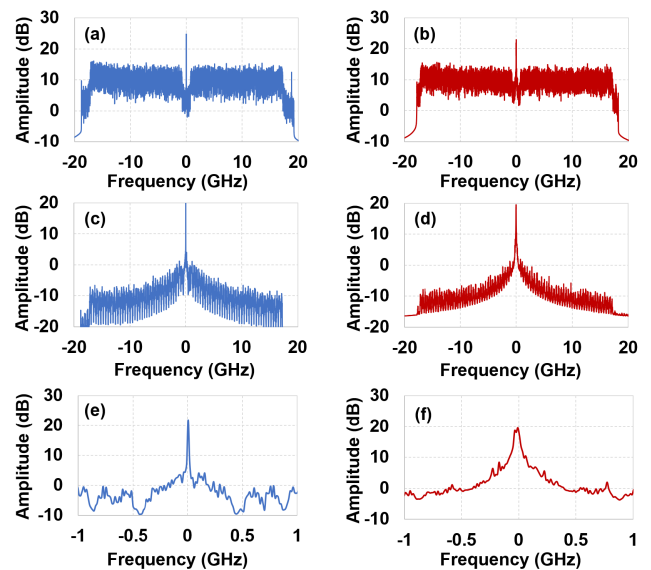

FIGURE 4. Spectrum of DMT signal for (a) ECL pair and (b) DFB pair. Spectrum of DMT signal after passing through the MAF for (c) ECL pair, (d) DFB pair, (e) ECL pair with enlarged details and (f) DFB pair with enlarged details.

Then we optimize several factors in the experimental demonstration and DSP-3 at back-to-back case. Figure 5(a) shows the BER performances versus bias voltage considering both ECL and DFB pairs. From Fig. 5(a), we can see that the BER is lowest when the bias voltage is 3.6 V for both cases. It is also noted that the performances degrade seriously when the MZM is biased exactly at the linear or null point. The optimal bias voltage is more close to the null point by considering the trade-off between the effective SNRs of signal and the accuracy of extracted phase information. Under fixed
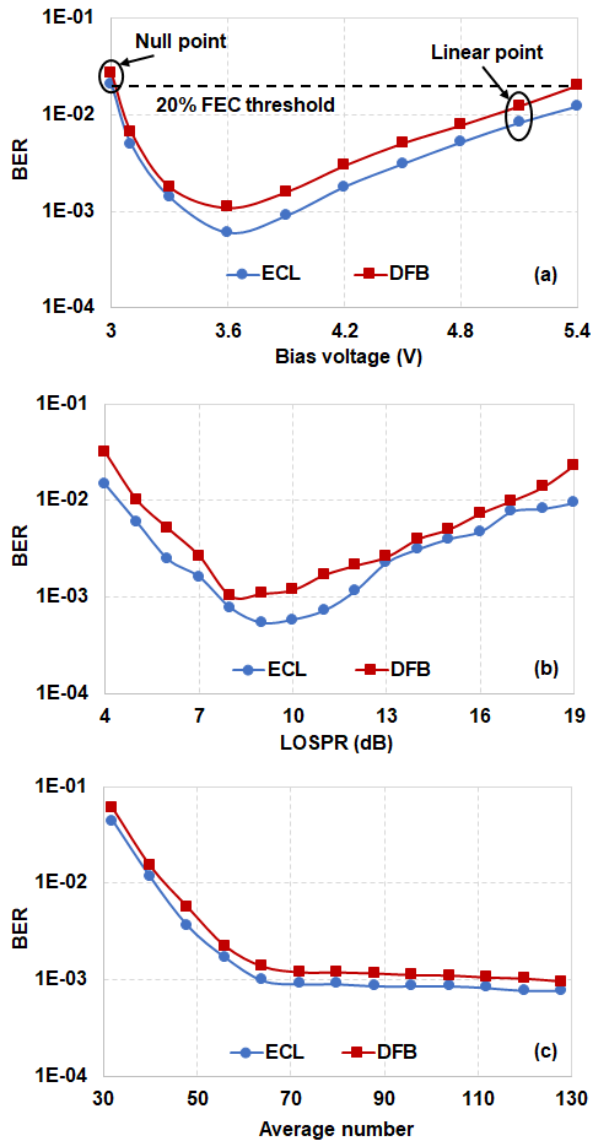
FIGURE 5. BER performances of ECL and DFB pairs at back-to-back versus (a) bias voltage, (b) power ratio between LO and DMT signal, and (c) average number in MAF.

power condition, the carrier-to-signal power ratio (CSPR) can be tuned by different value of bias voltage. It is noted that too large power of carrier may reduce the effective SNR of DMT signal. However, the accuracy of extracted carrier phase information will be seriously affected by the noise if the carrier power is too small. Considering the receiver structure based on single-end PD, the power ratio between LO and optical DMT signal should also be optimized. Figure 5(b) shows the BER performance versus LO-to-signal power ratio (LOSPR) for the ECL and DFB pairs. Here, we use the term "LOSPR" instead of term "CSPR" to distinguish our scheme from conventional direct detection scheme [25]. It is indicated in Fig. 5(b) that the optimal value of LOSPR can be viewed as 9 dB for both ECL and DFB pairs. Another important factor associated with the performance is the length of MAF in DSP-3. As shown in Fig. 5(c), the BER can

reach the stable performance when the length of MAF is larger than 72. However, in order to remove the operation of multiplication, the length is preferred to be the power of 2, which is 128 in our case. According to the results in Fig. 5, we use the optimized parameters in the future investigations.

Next, we compare the performances of 5 DSP schemes at back-to-back case. It is shown in Fig. 6(a) that the performances are similar among DSP-2 to DSP-5 schemes in ECL pairs. Because noise mitigation operation is not performed in DSP-1 scheme, the performance of DSP-1 scheme is much worse than those of other DSP schemes. It is also noted that the performance degradation of DSP-1 scheme is larger than 3 dB, which not follows the fact of 3 dB noise reduction in the previous analysis. This is mainly caused by the inaccurate channel estimation process if the noise in the training symbols is not mitigated. Considering the DSP-1 and DSP-2 schemes in Fig. 3, we believe that the frequency-domain noise mitigation in DSP-2 can also cancel the noise due to inaccurate channel estimation, which result in more than 3-dB performance improvement.

Figure 6(b) gives the performances of 5 DSP schemes with DFB pairs. It can be seen that both DSP-1 and DSP-2 schemes cannot recovery the signal. This is because the laser phase noise due to large laser linewidth cause large inter-carrier interference (ICI), which cannot be removed by traditional PNC algorithm. Again, DSP-3 and DSP-5 have similar performances. It is also shown that DSP-4 has a little better performance (less than 1 dB at BER of 0.02) than DSP-3 and DSP-5. This is mainly because DSP-3 and DSP-5 completely remove the imaginary part of the DMT signal, which will result in small nonlinear distortions especially if non-negligible residual phase noise exists after time-domain phase noise mitigation. To further prove the superiority of MAF-PNC, we investigate the estimated phase noise obtained from DSP-1 and DSP-3 in ECL pair, respectively. As shown in Fig. 6(c), the trends of estimated phase noise for the two cases are similar. However, traditional PNC algorithm assumes the phase noise is constant within one DMT symbol, which may introduce more deviations than MAF-PNC. The constellation points of the 5 DSP schemes based on both ECL and DFB pairs at OSNR of 32 dB are shown in Fig. 7, which also agree well with the results in Fig. 6. The constellation points cannot be clearly seen when DSP-1 and DSP-2 are applied on the case of DFB pair.

The fiber transmission performances of the 5 DSP schemes are also evaluated, which are shown in Fig. 8. At the transmission distance of 1040 km, the schemes of DSP-2 and DSP-4 shows a little better performances than DSP-3 and DSP-5 when ECL pair is used, as shown in Fig. 8(a). The BERs of DSP-2 and DSP-4 are $\sim 5 \times 10^{-4}$ at the optimal launch power of 1 dBm and the BERs of DSP-3 and DSP-5 are $\sim 6.9 \times 10^{-4}$ at the optimal launch power of 0 dBm. It can be explained that the nonlinear phase noise generated in the low-frequency region after long-haul transmission may reduce the phase noise estimation accuracy based on MAF, which will result in small nonlinear distortions after removing
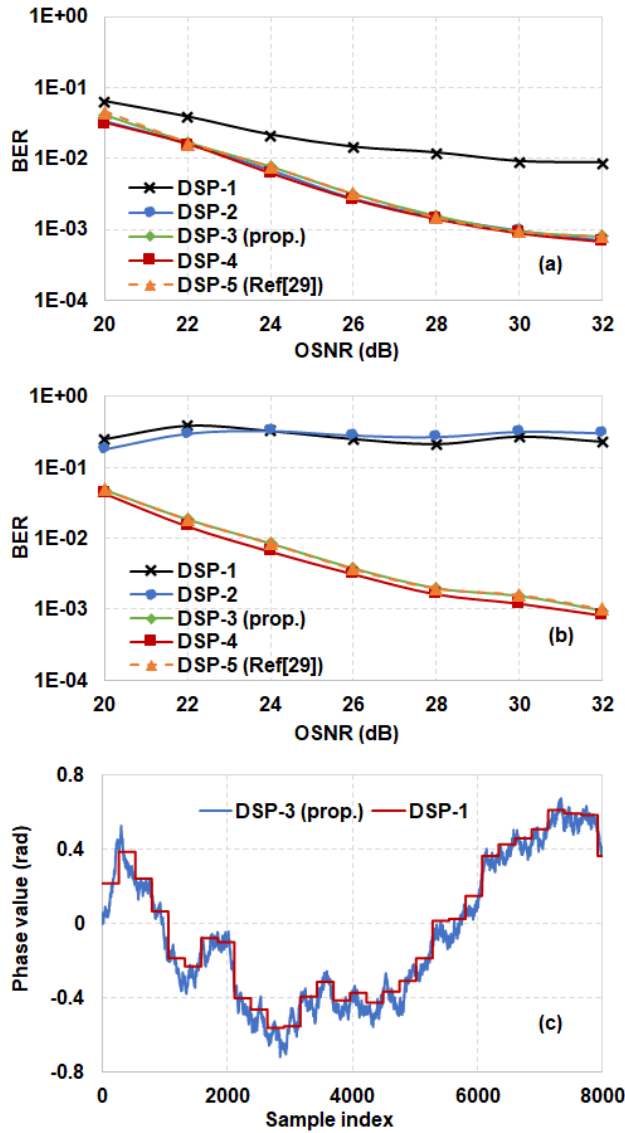
FIGURE 6. BER performances of 5 DSP schemes for (a) ECL and (b) DFB pairs at back-to-back case. (c) estimated phase curve based on DSP-1 and DSP-3.

FIGURE 7. Constellation points of 5 DSP schemes for ECL and DFB pairs.

the imaginary part of the DMT signal. When DFB pair is used, the result is similar to the back-to-back case. As also can be seen in Fig. 8(b), DSP-1 and DSP-2 schemes cannot recovery the signal, and DSP-4 scheme again shows a little better performance than DSP-3 and DSP-5 after 1040-km SSMF transmission. The BERs of DSP-4 are $\sim 3 \times 10^{-3}$ at the optimal launch power of 0 dBm and the BERs of DSP-3 and DSP-5 are $\sim 3.8 \times 10^{-3}$ at the same launch power. From Fig. 8(a) and (b), we can see that the optimal launch power is 1 dBm and 0 dBm for ECL and DFB pairs, respectively.

The BER performances versus transmission distance are also evaluated at the optimal launch power condition for the ECL and DFB pairs. It can be seen in Fig. 9(c) that the maximal transmission distance can be more than 1920 km at BER threshold of 0.02 when ECL pair and schemes of DSP-2 to DSP-5 are used. For the case of DFB pair shown
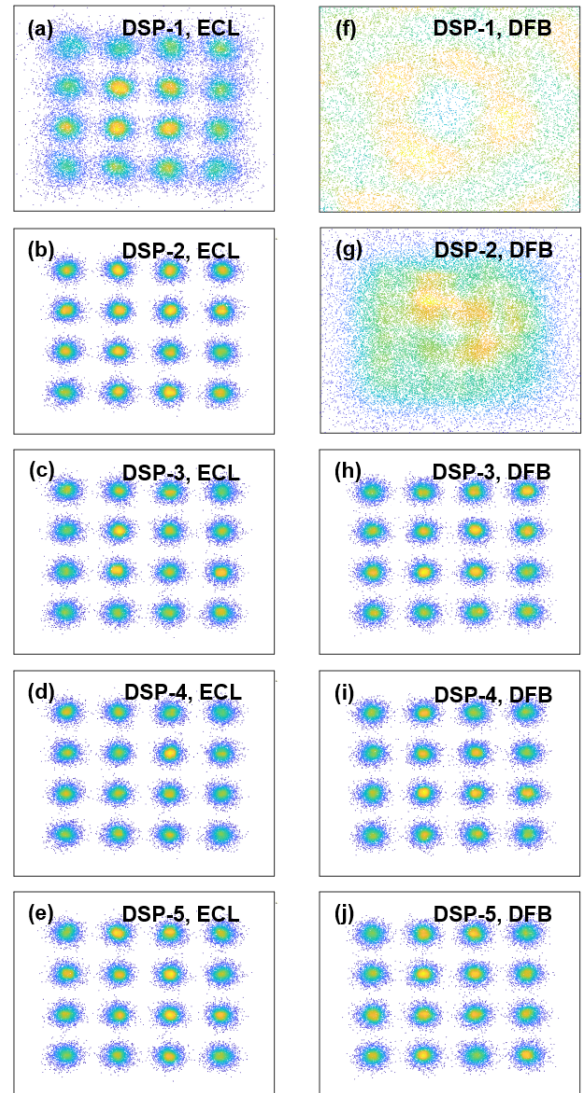
in Fig. 8(d), the maximal transmission distances for DSP-3 to DSP-5 are limited to be 1920 km, which are mainly affected by increasing linear and nonlinear phase noise.

Finally, we briefly compare the computational complexity of the DSP schemes in terms of complex multiplication operations considering only the PNC and CE/E steps. In the calculation, we define N_{sc}, N_{fft}, N_{sym} and N_{cp} as the number of used subcarriers, FFT size, symbol and CP length, which are 152, 256, 320 and 8 in our experimental case. The number of complex multiplication operations per DMT symbol for all the 5 DSP schemes are described in Table 1. We first consider the CE/E steps. For DSP-1, DSP-3 and DSP-5, the signals before FFT demodulation is real-valued. Therefore, half of the used subcarriers are sufficient for signal recovery since DMT signal is encoded in symmetrical conjugation manner. For DSP-2 and DSP-4, however, the signals before FFT demodulation is complex-valued and the effective SNR enhancement is performed in frequency domain. In this case,
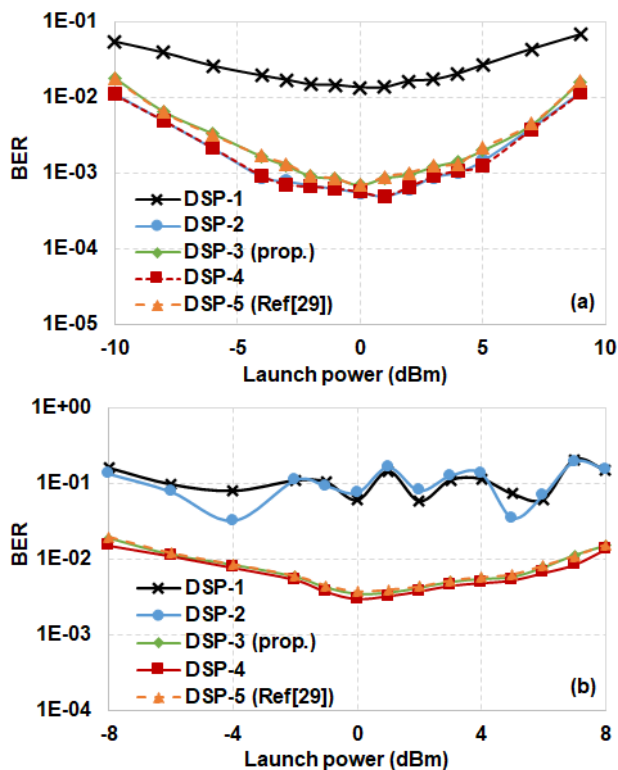
FIGURE 8. BER performances of 5 DSP schemes versus launch power after 1040-km SSMF transmission for (a) ECL and (b) DFB.

FIGURE 9. BER performances of 5 DSP schemes versus transmission distance at launch power of 0 dBm for (a) ECL and 1 dBm for (b) DFB.

all the used subcarriers have to be processed, resulting in the double of the number of complex multiplication operations.

For the PNC step, DSP-1 and DSP-2 assume same common phase error (CPE) in one DMT symbol. Therefore, the required number of complex multiplications for these two DSP schemes are only related to the processed subcarriers, as described in Table 1. DSP-3 and DSP-4 compensate the phase noise in time domain in a sample-to-sample case. Therefore, the number of complex multiplication operations is related to the length of one DMT symbol, which is equal to the value of $N_{fft} + N_{cp}$. It is noted that the complex multiplication operations are not required in the phase noise estimation process according to previous analysis. In Table 1, the factor *2* for DSP-3 and DSP-4 represents the normalization and compensation process shown in Fig. 1(a).

TABLE 1. Number of complex multiplication operations per DMT symbol in the CE/E and PNC steps for schemes from DSP-1 to DSP-5.

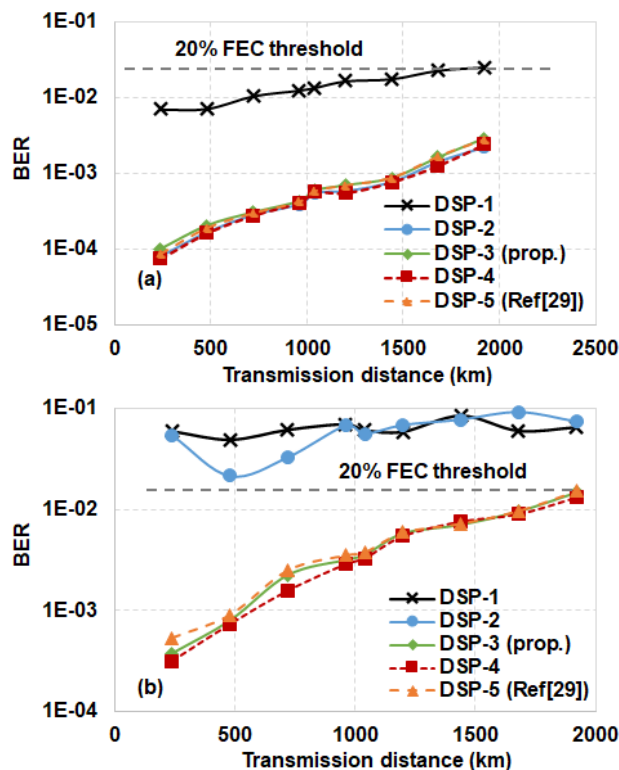| Scheme	CE/E	PNC
DSP-1	$N_{sc}/2 = 76$	$N_{sc}/2 = 76$
DSP-2	$N_{sc} = 152$	$N_{sc} = 152$
DSP-3	$N_{sc}/2 = 76$	$2 \times (N_{fft} + N_{cp}) = 528$
DSP-4	$N_{sc} = 152$	$N_{sc} + 2 \times (N_{fft} + N_{cp}) = 680$
DSP-5	$N_{sc}/2 = 76$	$2 \times (N_{fft} + N_{cp}) \times log_2[N_{sym} \times (N_{fft} + N_{cp})] + 2 \times (N_{fft} + N_{cp}) \approx 9000$

Since CPE compensation is also implemented in DSP-4, another N_{sc} complex multiplication operations are required for each DMT symbol. For DSP-5, the operations of complex multiplication includes two parts. The first part represents the FFT and IFFT operations, which are implemented on the whole signal block with length of $N_{sym} \times (N_{fft} + N_{cp})$. The factor *2* means both FFT and IFFT operations are required to extract the phase information in time domain. The second part represents the two absolute value operations (Eq. (4) in [29]) to remove the imaginary noise. As shown in Table 1, DSP-5 requires much more complex multiplication operations than other DSP schemes. According to the results from Fig. 4 to Fig. 9, it can be concluded that DSP-3 combining time-domain PNC and imaginary part removal has the best performance in terms of low computational complexity and large tolerance to noise.

V. CONCLUSION

We have proposed a simple noise mitigation scheme combining time-domain PNC and imaginary part removal in the coherent optical DMT transmission system based on low complex structure. Through the proof-of-concept experimental demonstration, we find our proposed scheme superior to other schemes by providing both lowest computational complexity and larger laser phase noise tolerance. The experimental results indicate that the proposed scheme can support laser linewidth as large as 10 MHz and 1920-km SSMF transmission. We believe our proposed DSP scheme may have

great potential in future low-cost and low-complexity fibre network scenarios such as datacentre inter/intra-connections and coherent passive optical network.

REFERENCES

[1] T. Kobayashi, M. Nakamura, F. Hamaoka, M. Nagatani, H. Yamazaki, H. Nosaka, and Y. Miyamoto, "Long-haul WDM transmission with over-1-Tb/s channels using electrically synthesized high-symbol-rate signals," in *Proc. Opt. Fiber Commun. Conf. (OFC)*, 2020, pp. 1–3.

[2] T. Kobayashi, M. Nakamura, F. Hamaoka, M. Nagatani, H. Wakita, H. Yamazaki, T. Umeki, H. Nosaka, and Y. Miyamoto, "35-Tb/s C-band transmission over 800 km employing 1-Tb/s PS-64QAM signals enhanced by complex 8 × 2 MIMO equalizer," in *Proc. Opt. Fiber Commun. Conf. Postdeadline Papers*, 2019, pp. 1–3.

[3] P. J. Winzer, D. T. Neilson, and A. R. Chraplyvy, "Fiber-optic transmission and networking: The previous 20 and the next 20 years," *Opt. Express*, vol. 26, no. 18, pp. 24190–24239, 2018.

[4] X. Miao, M. Bi, Y. Fu, L. Li, and W. Hu, "Experimental study of NRZ, duobinary, and PAM-4 in O-Band DML-based 100G-EPON," *IEEE Photon. Technol. Lett.*, vol. 29, no. 17, pp. 1490–1493, Sep. 1, 2017.

[5] Z. Tan, C. Yang, Y. Zhu, Z. Xu, K. Zou, F. Zhang, and Z. Wang, "High speed band-limited 850-nm VCSEL link based on time-domain interference elimination," *IEEE Photon. Technol. Lett.*, vol. 29, no. 9, pp. 751–754, May 1, 2017.

[6] R. Lin, X. Pang, J. Van Kerrebrouck, M. Verplaetse, O. Ozolins, A. Udalcovs, L. Zhang, L. Gan, M. Tang, S. Fu, R. Schatz, U. Westergren, S. Popov, D. Liu, W. Tong, T. De Keulenaer, G. Torfs, J. Bauwelinck, X. Yin, and J. Chen, "Real-time 100 Gbps/λ/core NRZ and EDB IM/DD transmission over 10 km multicore fiber," in *Proc. Opt. Fiber Commun. Conf.*, 2018, pp. 1–3.

[7] Z. Yang, F. Gao, S. Fu, X. Li, L. Deng, Z. He, M. Tang, and D. Liu, "Radial basis function neural network enabled C-band 4×50 Gb/s PAM-4 transmission over 80 km SSMF," *Opt. Lett.*, vol. 43, no. 15, pp. 3542–3545, 2018.

[8] J. Zhang, T. Ye, X. Yi, C. Yu, and K. Qiu, "An efficient hybrid equalizer for 50 Gb/s PAM-4 signal transmission over 50 km SSMF in a 10-GHz DML-based IM/DD system," in *Proc. Conf. Lasers Electro-Optics*, 2017, pp. 1–3.

[9] M. He, M. Xu, Y. Ren, J. Jian, Z. Ruan, Y. Xu, S. Gao, S. Sun, X. Wen, L. Zhou, L. Liu, C. Guo, H. Chen, S. Yu, L. Liu, and X. Cai, "High-performance hybrid silicon and lithium niobate Mach-Zehnder modulators for 100 Gbit s-1 and beyond," *Nature Photon.*, vol. 13, no. 5, pp. 359–364, 2019.

[10] M. Li, L. Wang, X. Li, X. Xiao, and S. Yu, "Silicon intensity Mach–Zehnder modulator for single lane 100 Gb/s applications," *Photon. Res.*, vol. 6, no. 2, pp. 109–116, 2018.

[11] Y. Zhu, F. Zhang, F. Yang, L. Zhang, X. Ruan, Y. Li, and Z. Chen, "Toward single lane 200G optical interconnects with silicon photonic modulator," *J. Lightw. Technol.*, vol. 38, no. 1, pp. 67–74, Jan. 1, 2020.

[12] S. Zhou, X. Li, L. Yi, Q. Yang, and S. Fu, "Transmission of 2×56 Gb/s PAM-4 signal over 100 km SSMF using 18 GHz DMLs," *Opt. Lett.*, vol. 41, no. 8, pp. 1805–1808, 2016.

[13] K. Yonenaga and N. Takachio, "A fiber chromatic dispersion compensation technique with an optical SSB transmission in optical homodyne detection systems," *IEEE Photon. Technol. Lett.*, vol. 5, no. 8, pp. 949–951, Aug. 1993.

[14] S. R. Blais and J. Yao, "Optical single sideband modulation using an ultranarrow dual-transmission-band fiber Bragg grating," *IEEE Photon. Technol. Lett.*, vol. 18, no. 21, pp. 2230–2232, Nov. 2006.

[15] X. Li, S. Zhou, H. Ji, M. Luo, Q. Yang, L. Yi, R. Hu, C. Li, S. Fu, A. Alphones, W.-D. Zhong, and C. Yu, "Transmission of 4×28-Gb/s PAM-4 over 160-km single mode fiber using 10G-class DML and photodiode," in *Proc. Opt. Fiber Commun. Conf.*, 2016, pp. 1–3.

[16] Z. Li, L. Yi, X. Wang, and W. Hu, "28 Gb/s duobinary signal transmission over 40 km based on 10 GHz DML and PIN for 100 Gb/s PON," *Opt. Express*, vol. 23, no. 16, pp. 20249–20256, 2015.

[17] L. Xue, L. Yi, W. Hu, R. Lin, and J. Chen, "Optics-simplified DSP for 50 Gb/s PON downstream transmission using 10 Gb/s optical devices," *J. Lightw. Technol.*, vol. 38, no. 3, pp. 583–589, Feb. 1, 2020.

[18] N. Eiselt, J. Wei, H. Griesser, A. Dochhan, M. Eiselt, J.-P. Elbers, J. J. V. Olmos, and I. T. Monroy, "First real-time 400G PAM-4 demonstration for inter-data center transmission over 100 km of SSMF at 1550 nm," in *Proc. Opt. Fiber Commun. Conf.*, 2016, pp. 1–3.

[19] X. Dai, X. Li, M. Luo, Q. You, and S. Yu, "LSTM networks enabled nonlinear equalization in 50-Gb/s PAM-4 transmission links," *Appl. Opt.*, vol. 58, no. 22, pp. 6079–6084, 2019.

[20] P. Zhu, J. Li, P. Zhou, B. Lin, Z. Chen, and Y. He, "Upstream WDM-PON transmission scheme based on PDM-OOK modulation and digital coherent detection with dual-modulus algorithm," *Opt. Express*, vol. 23, no. 10, pp. 12750–12757, 2015.

[21] J. Zhang, J. Yu, X. Li, K. Wang, W. Zhou, J. Xiao, L. Zhao, X. Pan, B. Liu, and X. Xin, "200 Gbit/s/λ PDM-PAM-4 PON system based on intensity modulation and coherent detection," *J. Opt. Commun. Netw.*, vol. 12, no. 1, p. A1, 2020.

[22] H. Xin, D. Kong, K. Zhang, S. Jia, Y. Fu, W. Hu, and H. Hu, "100 GBPS simplified coherent PON using carrier-suppressed PDM-PAM-4 and phase-recovery-free KK detection," in *Proc. 45th Eur. Conf. Opt. Commun. (ECOC)*, 2019, pp. 1–3.

[23] C. Li, M. Luo, and X. Li, "4× 128-Gb/s PDM-DMT signal transmission over 1440-km SSMF with high phase noise tolerance," *Opt. Express*, vol. 26, no. 23, pp. 30901–30910, 2018.

[24] W.-R. Peng, T. Tsuritani, and I. Morita, "Simple carrier recovery approach for RF-pilot-assisted PDM-CO-OFDM systems," *J. Lightw. Technol.*, vol. 31, no. 15, pp. 2555–2564, Aug. 2013.

[25] Z. Li, M. S. Erkilinc, K. Shi, E. Sillekens, L. Galdino, B. C. Thomsen, P. Bayvel, and R. I. Killey, "SSBI mitigation and the Kramers–Kronig scheme in single-sideband direct-detection transmission with receiver-based electronic dispersion compensation," *J. Lightw. Technol.*, vol. 35, no. 10, pp. 1887–1893, May 15, 2017.

[26] T. M. Schmidl and D. C. Cox, "Robust frequency and timing synchronization for OFDM," *IEEE Trans. Commun.*, vol. 45, no. 12, pp. 1613–1621, 1997.

[27] X. Liu, F. Buchali, and R. W. Tkach, "Improving the nonlinear tolerance of polarization-division-multiplexed CO-OFDM in long-haul fiber transmission," *J. Lightw. Technol.*, vol. 27, no. 16, pp. 3632–3640, Aug. 2009.

[28] X. Yi, W. Shieh, and Y. Ma, "Phase noise effects on high spectral efficiency coherent optical OFDM transmission," *J. Lightw. Technol.*, vol. 26, no. 10, pp. 1309–1316, May 2008.

[29] C. Li, R. Hu, Q. Yang, M. Luo, W. Li, and S. Yu, "Fading-free transmission of 124-Gb/s PDM-DMT signal over 100-km SSMF using digital carrier regeneration," *Opt. Express*, vol. 24, no. 2, pp. 817–824, 2016.

KE LI received the Ph.D. degree in systems engineering from the Naval University of Engineering, Wuhan, China, in 2013. He is currently an Deputy Director of the department working in the Naval University of Engineering. His research interests include data fusion, target detection, and recognition in communication systems.

TIANYE HUANG (Member, IEEE) received the M.Sc. and Ph.D. degrees from the Huazhong University of Science and Technology. From 2013 to 2016, he joined the Photonics Institute, Nanyang Technology University, as a Research Fellow. Then, he became a Professor with the School of Mechanical Engineering and Electronic Information, China University of Geosciences. His research interest focuses on nonlinear optics and optical communications.

ZHONG LIU received the Ph.D. degree in control science and engineering from the Huazhong University of Science and Technology, Wuhan, China, in 1998. He is currently an Professor with the Weapon Engineering College, University of Navy Engineering, Wuhan. His research interests include data fusion and automatic control.

QIANQIAN LIU received the Ph.D. degree in control science and engineering from the Huazhong University of Science and Technology, Wuhan, China, in 1998. He is currently an Professor with the Weapon Engineering College, University of Navy Engineering, Wuhan. His research interests include data fusion and automatic control.

YUNLEI ZHANG (Member, IEEE) was born in Hebei, China, in 1981. He received the B.S. and M.S. degrees from Navy Engineering University, Wuhan, China, in 2004 and 2007, respectively, and the Ph.D. degree from the Department of Electronic Engineering, Tsinghua University, in 2020. His research interests mainly include MIMO radar signal processing and software radar signal processing.

LIGUO LIU was born in 1983. He received the bachelor's degree in physics, the master's degree in quantum information, and the Ph.D. degree in electromagnetic field and microwave techniques from the National University of Defense Technology, in 2002, 2008, and 2013, respectively. He is currently a Lecturer with the Naval University of Engineering Technology. His research interests include electromagnetic analysis, parallel computation, and meta-materials.

LU LI was born in Hubei, China, in 1986. She received the bachelor's and master's degrees from the Wuhan University of Technology, in 2009 and 2012, respectively. Her research interests mainly include computer technology, and data analysis and processing.

XIANG LI received the M.Sc. degree from the School of Optical and Electronic Information, Huazhong University of Science and Technology, in July 2011, and the Ph.D. degree from the School of Electrical and Electronic Engineering, Nanyang Technology University, in May 2016. Then, he became a Senior Research Engineer with the Wuhan Research Institute of Posts and Telecommunications. In October 2019, he joined the Electrical Engineering Department, University of Cambridge, as a Senior Research Associate. His research interest focuses on digital signal processing for high-speed coherent optical transmission systems.

• • •